Nano Energy 105 (2023) 108007

Contents lists available at ScienceDirect

Nano Energy

journal homepage: www.elsevier.com/locate/nanoen

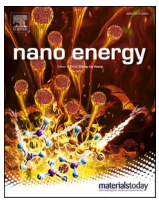

A bioinspired ionic diode membrane based on sub-2 nm covalent organic framework channels for ultrahigh osmotic energy generation

Mengyao Gao [a,1], Min-Jie Zheng [a,1], Ahmed F.M. EL-Mahdy [b,1], Chen-Wei Chang [a], Yu-Chun Su [a], Wen-Hsin Hung [a], Shiao-Wei Kuo [b,c,*], Li-Hsien Yeh [a,d,**]

[a] Department of Chemical Engineering, National Taiwan University of Science and Technology, Taipei 10607, Taiwan
[b] Department of Materials and Optoelectronic Science, Center of Crystal Research, National Sun Yat-Sen University, Kaohsiung 80424, Taiwan
[c] Department of Medicinal and Applied Chemistry, Kaohsiung Medical University, Kaohsiung 807, Taiwan
[d] Center of Automation and Control, National Taiwan University of Science and Technology, Taipei 10607, Taiwan

ARTICLE INFO

Keywords:
Nanofluidics
Ion selectivity
COF membrane
One-dimensional nanochannels
Osmotic energy harvesting
Ion current rectification

ABSTRACT

Electric eels can convert ionic concentration gradients into a high-efficiency power via a large number of sub-2 nm transmembrane ion channels, which can exhibit high ion selectivity and strong diode-like ion rectification property. Inspired by this, herein, we report on a sub-2 nm scale ionic diode membrane, composed of an ultrathin (~110 nm) β-ketoenamine-linked two-dimensional covalent-organic framework (COF) membrane and a highly ordered alumina nanochannel membrane (ANM), for highly efficient osmotic energy harvesting. As verified by our experimental and simulation results, the heterostructured membrane with the features of asymmetric charges and pore sizes in two aligned COF (1.1 nm) and ANM (100 nm) channels is capable of highly rectifying ion transport even in high 0.5 M salt solution. Benefiting from the presence of abundant sub-2 nm COF-based ion channels and the strong ionic diode effect, an unprecedented power density of up to 27.8 W/m^2 is achieved by mixing the artificial salt-lake water and river water (500-fold NaCl gradient). This study will open new avenues of using the rectified ion channel-mimetic nanofluidic membrane as a new platform towards the exploration and development of an ultrahigh osmotic power generator.

1. Introduction

With the ever-increasing demand of energy, the development of efficient, renewable, and environmentally friendly energy sources is in an imperative need. Among the explored clean energies, the chemical energy existing in a salinity gradient, the so-called osmotic energy [1,2] or blue energy [3], has recently drawn incremental attention due to the ultrahigh theoretical energy capacity (~0.8 kWh/m^3) that can be produced when seawater is mixed with river water. In order to capture this type of clean energy in a more efficient way, significant efforts on developing the reverse electrodialysis (RED)-based ion-selective membranes with nanoscale channels [4–12] have been made. However, these existing RED membranes suffer from inferior ion selectivity and insufficient ionic flux [13], leading to the poor osmotic energy conversion performance. This is expected because the Debye length at the salt (e.g., NaCl or KCl) concentration simulating the seawater (~0.5 M) that is commonly used in osmotic energy conversion is about 0.43 nm [14], which is much smaller than the pore size (ca. 5–20 nm) used in those existing nanofluidic membranes. As to enhance the ion selectivity, the membranes with sub-2 nm-scale (or even subnanometer-scale) pores/channels have been developed. For example, considerable efforts have been made on the two-dimensional (2D) nanofluidic membranes [15], composed of highly ion-selective and sub-2 nm channels through the assembly of 2D lamellar materials. But the advancement of the osmotic energy harvesting performance using 2D lamellar membranes is still limited owing to high resistance from their highly tortuous ion pathways [16–19].

Electric eels can realize highly efficient osmotic energy harvesting by utilizing numerous transmembrane asymmetric ion channels on their electrocytes [20], and when being stimulated these sub-2 nm channels

* Corresponding author at: Department of Materials and Optoelectronic Science, Center of Crystal Research, National Sun Yat-Sen University, Kaohsiung 80424, Taiwan.
** Corresponding author at: Department of Chemical Engineering, National Taiwan University of Science and Technology, Taipei 10607, Taiwan.
E-mail addresses: kuosw@faculty.nsysu.edu.tw (S.-W. Kuo), lhyeh@mail.ntust.edu.tw (L.-H. Yeh).
[1] These authors contributed equally to this work

https://doi.org/10.1016/j.nanoen.2022.108007
Received 31 August 2022; Received in revised form 21 October 2022; Accepted 10 November 2022
Available online 11 November 2022

behave like an ionic diode, capable of achieving unidirectional and amplified ion transport [21–23] (Fig. 1a). Nanofluidics with such diode-like rectification property has been shown as promising platform for improving osmotic energy harvesting [24–26]. Motivated by this, a series of ionic diode membranes have been designed to harvest osmotic energy with enhanced efficiency [27–34]. For example, Gao et al. pioneered the ionic diode membrane made of mesoporous carbon (with pore size of ~7 nm) and macroporous alumina channels (with pore size of ~80 nm), achieving a high power density of 3.46 W/m^2 [27]. Followed by this design concept, Zhou et al. developed the mesoporous carbon-silica/anodized aluminum oxide ionic diode membrane, which reached the best rectification ratio of 3.82 at 1 mM KCl and achieved the power output of 5.04 W/m^2 [28]. However, so far most of the state-of-the-art ionic diode membranes are made from nanoscale channels [27–34], limiting ion selectivity and advancement in power output. Moreover, it has been shown that the design of membranes based on the ordered and connected channel structure is capable of decreasing resistance and promoting permeability, thus enhancing osmotic energy conversion efficiency [35,36]. As a consequence, to strive for higher power output, the exploitation of the ionic diode membrane with ordered sub-2 nm channels is highly desirable.

Covalent-organic frameworks (COFs), with the advantages of high porosity of small pores (<5 nm) and uniformly aligned one-dimensional (1D) channels, have drawn extensive attention in separation, purification and energy researches [37–39]. The free-standing COF-based membranes have been shown to be a promising candidate in highly efficient osmotic energy harvesting [40–46], because they can offer abundant aligned 1D nanochannels, which can reduce pathways for ion transport, resulting in decreased membrane resistance. However, to the best of our knowledge, the high-performance COF-based ionic diode membrane for harvesting energy from salinity gradients have yet been reported.

Inspired by the nanoarchitecture and biological function of ion channels in the electric eel, herein for the first time we report a sub-2 nm-scale ionic diode membrane (denoted as TFP-TPA COF@ANM), composed of an ultrathin (~110 nm) 2D β-ketoenamine-linked COF (TFP-TPA COF; pore size ~1.1 nm) membrane and an alumina nanochannel membrane (ANM; pore size ~100 nm;), for enhancing osmotic energy harvesting (Fig. 1a,b). The TFP-TPA COF thin film was synthesized through a facile Schiff-base reaction [47] via the interfacial polymerization of 1,3,5-triformylphloglucinol (TFP) and tris (4-aminophenyl)amine (TPA-3NH$_2$) (Fig. 1b; see details in Experimental section). The design of asymmetric surface charges and ordered micro- to macroporous structure endow the COF-based ionic diode membrane proposed with high rectification ability even in the high 0.5 M salt environment simulating seawater condition. A large number of sub-2 nm transmembrane ion channels formed by π-π stacking of TFP-TPA COF (Fig. 1c) render the heterogeneous membrane highly selective and efficient for ion transport. Benefiting from the above two reasons, the sub-2 nm-scale COF-based ionic diode membrane reported is capable of achieving an unprecedented power output of up to 27.8 W/m^2 in hypersaline environment (5 M/0.01 M NaCl gradient), surpassing all the reported RED-based membranes under the same testing condition.

2. Results and discussion

The fabrication of the sub-2 nm-scale ionic diode membrane, TFP-TPA COF@ANM, was performed through two facial stages (Fig. 1b). Firstly, the TFP-TPA COF membrane was synthesized by using the trialdehyde linker TFP in dichloromethane as a bottom-organic layer and the tri-amino linker TPA-3NH$_2$ with p-toluenesulfonic acid in deionized water and acetonitrile as an up-aqueous layer. The Schiff-base reaction between TFP and TPA-NH$_2$ was carried out at the two-layer interface via a slow diffusion process of the two linkers, then forming the orange TFP-TPA COF membrane (Fig. S1). The ANM was fabricated by the two-step anodization process in oxalic acid and one further step of pore widening in phosphoric acid (Fig. S2), modified from our previous publication [48]. In the second stage, the resulting TFP-TPA COF membrane was transferred onto the ANM surface, followed by thermal annealing at 80 °C for 3 days to confirm the immobilization of TFP-TPA COF thin film on the surface of ANM substrate (Fig. 1d). In view of a significant number of carbonyl and amine groups in TFP-TPA COF, numerous hydrogen bonds are formed on the interface between TFP-TPA COF and ANM, contributing to the enhanced robustness of the interface and stability in water.

The successful fabrication of the sub-2 nm-scale heterogeneous membrane, TFP-TPA COF@ANM, was confirmed by using scanning electron microscopy (SEM), high-resolution transmission electron microscope (HRTEM), Fourier-transform infrared spectroscopy (FTIR), solid state nuclear magnetic resonance (NMR) spectroscopy, powder X-ray diffraction (PXRD), and N_2 adsorption-desorption isotherms (Fig. 2 and S3). The SEM morphology images shown in Fig. 2a-d clearly revealed that an ultrathin (~110 nm) TFP-TPA COF membrane was uniformly distributed on the ANM substrate (with a thickness of ~25 μm

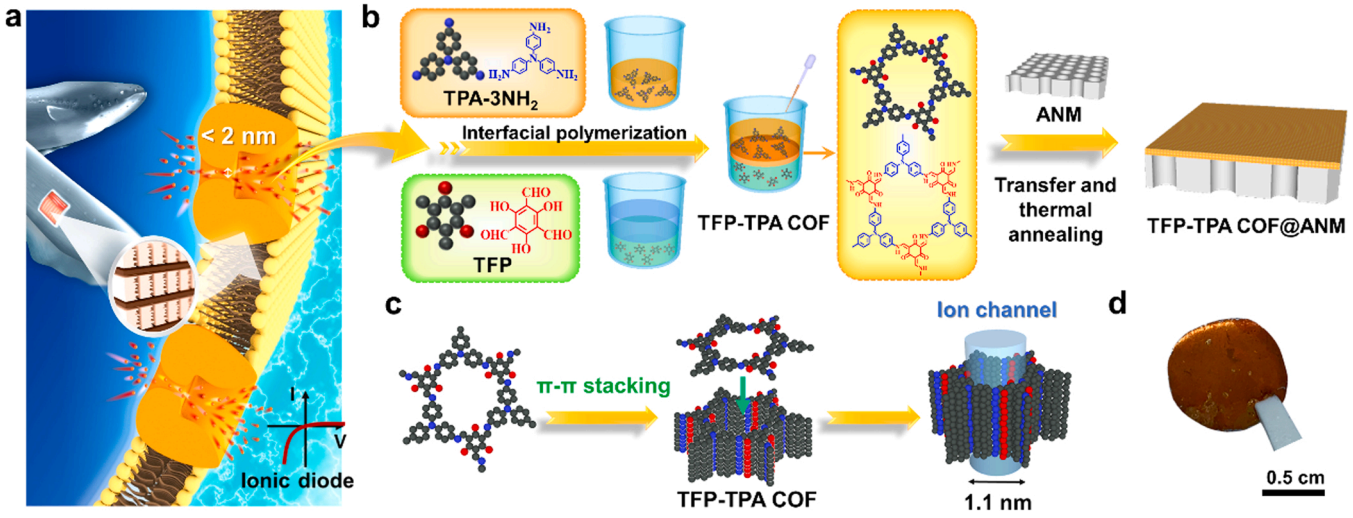

Fig. 1. Fabrication of a bioinspired ionic diode membrane, TFP-TPA COF@ANM. (a) Schematic representation of the electric eel-inspired sub-2 nm-scale ionic diode membrane for the amplification of energy harvesting from a salinity gradient. (b) Fabrication process of TFP-TPA COF@ANM via interfacial polymerization and thermal annealing. (c) Schematic of the formation of ordered sub-2 nm-scale ion channels in TFP-TPA COF membrane via the π-π stacking interaction. (d) Photograph of the prepared TFP-TPA COF@ANM.

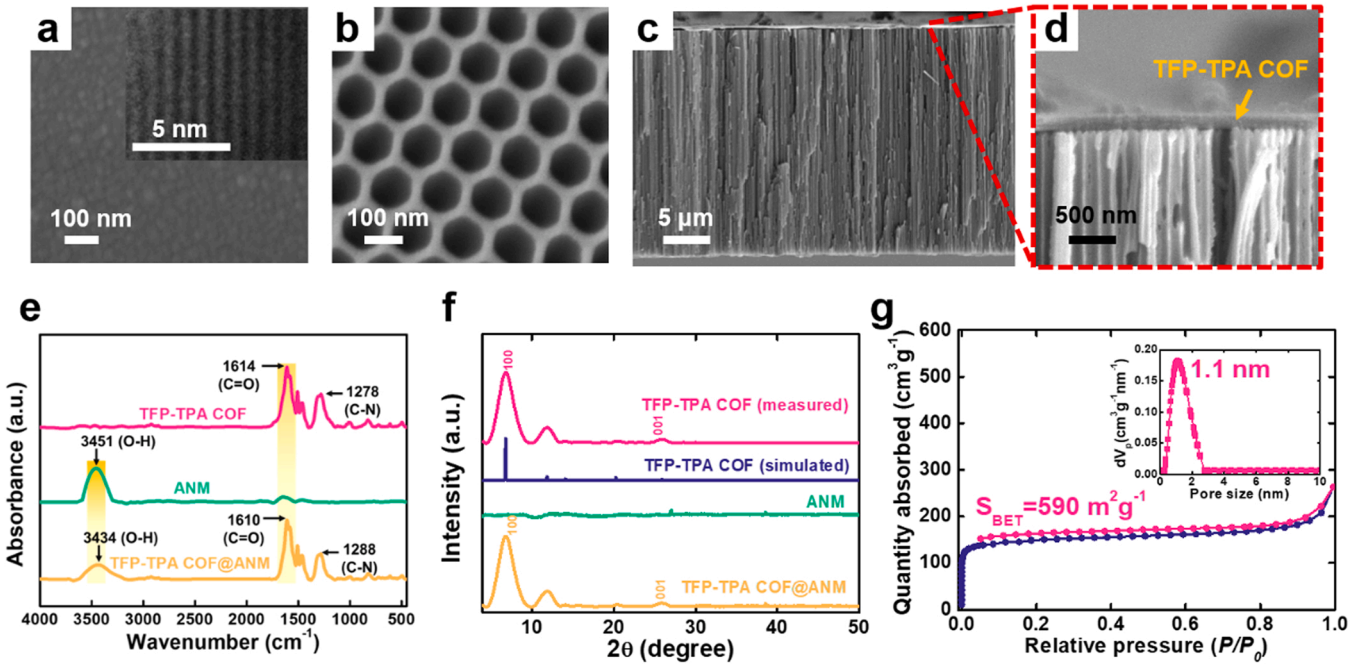

Fig. 2. Characterizations of TFP-TPA COF@ANM. SEM images of the (a) top view (COF side), (b) bottom view (ANM side), and (c) cross-section view of the TFP-TPA COF@ANM. The pore diameter and thickness of the ANM are about 100 nm and 25 μm, respectively. Inset in (a) reveals the HRTEM image of the TFP-TPA COF membrane, indicating its well-ordered crystalline structure. (d) Magnified cross-section view of the TFP-TPA COF membrane at the COF/ANM interface. The thickness of TFP-TPA COF membrane is ~110 nm. (e) FTIR and (f) PXRD measurements of TFP-TPA COF, ANM, and heterogeneous TFP-TPA COF@ANM. (g) N_2 adsorption and desorption isotherms of TFP-TPA COF, revealing that its BET surface area is ~590 m^2g^{-1}. Inset denotes the estimated nominal pore size distributions of TFP-TPA COF using the density functional theory (DFT) model, indicating a majority of uniform ~1.1 nm pore size of ion channels in TFP-TPA COF.

and highly uniform pore size of ~100 nm). The HRTEM image shown in the inset of Fig. 2a confirmed the well-oriented crystalline structure of TFP-TPA COF and the clear lattice fringes indicated the well-ordered nanochannels. The FTIR spectra of TFP-TPA COF, ANM and TFP-TPA COF@ANM also confirmed the chemical structures of the membranes prepared. As shown in Fig. 2e, the disappearance of aldehyde (CHO) and amino (NH_2) stretching bands and the appearance of a new C═C stretching band at 1583 cm^{-1}, C═O stretching band at 1614 cm^{-1}, and C-N stretching band at 1278 cm^{-1} confirmed the Schiff-base condensation between TFP and TPA-NH_2 linkers and the presence of the β-ketoenamine form in TFP-TPA COF membrane. Note that the strong OH stretching vibration of ANM was observed, and after attached a TFP-TPA COF membrane the OH peak become broader and the peak position was shifted from 3451 cm^{-1} to 3434 cm^{-1}. In addition, the C═O group at 1614 cm^{-1} of the TFP-TPA COF membrane was shifted to 1610 cm^{-1} after attached an ANM membrane, indicating that the intermolecular interaction such as hydrogen bonding may occur between the TFP-TPA COF membrane and ANM as expected. Furthermore, we also used the solid state ^{13}C NMR spectroscopy to confirm the fabrication of TFP-TPA COF (Fig. S3). The TFP-TPA COF membrane can be featured by the three signals, including 191.80 ppm for C═O group, 153.35 ppm for =C–NH group, and 114.45 ppm for C═C group, which are consistent with the β-ketoenamine form. The PXRD patterns shown in Fig. 2 f also confirmed the highly ordered pore structure of TFP-TPA COF and the successful fabricaiton of TFP-TPA COF@ANM. The experimental results was in good agreement with the simulated results from the eclipsed A-A stacking model. The most intense peak at the lowest 2θ value of ~6.78° can be attributed to the (100) plane with a pore aperture of ~1.3 nm, demonstrating the formation of ordered 1D sub-2 nm channels. The peak at the 2θ value of ~25.81° was ascribed to the (001) plane caused by the π-π stacking of TFP-TPA COF layers. The uniformly distributed sub-2 nm channels formed in TFP-TPA COF membrane was also demonstrated by N_2 adsorption/desorption isotherms, which indicated a majority of ~1.1 nm pores (close to the value of ~1.3 nm estimated by PXRD) with the high Brunauer-Emmett-Teller (BET) surface area of 590 m^2g^{-1} and a total pore volume of 0.35 cm^3g^{-1}. The hydrophility of TFP-TPA COF@ANM was demonstrated by the contact angle measurments (Fig. S4), proving its applicability in ionic device applications. The features of high specific surface area and high density of uniformly aligned sub-2 nm channels in 2D TFP-TPA COF and the highly ordered channel array in ANM endow the resulting heterogeneous membrane with high potential towards high-performance osmotic energy harvesting [35].

We first examined the ion transport property of the prepared sub-2 nm-scale heterogeneous membrane (TFP-TPA COF@ANM) by assembling it into a manmade conductive cell, which comprises two identical compartments filled with the same concentration of electrolyte [49]. Here, we used the KCl as working electrolyte because of the nearly the same diffusivities of K^+ and $C1^-$ ($\sim 2 \times 10^{-9} m^2/s$). As shown in Fig. 3a, in all KCl concentrations considered, the TFP-TPA COF@ANM revealed significant nonlinear diode-like ion current rectification (ICR) property [21] such that currents at negative voltage were significantly higher than currents at positive voltage of the same magnitude. Without ANM, the pure TFP-TPA COF membrane showed linear Ohmic behavior (Fig. S5), indicating that the incorporation of the ANM into the heterogeneous membrane induces the ICR property. Most importantly, even at high salt concentration of 0.5 M simulating seawater condition, the TFP-TPA COF@ANM still rectified ionic current with a high rectification ratio of about 10, indicating the realization of a high-performance sub-2 nm-scale ionic diode membrane. The strong ICR property can be attributed to the net effects of the creation of asymmetric surface charges (negatively charged for TFP-TPA COF (Fig. S6) and positively charged for ANM [48]) and pore sizes of aligned nanofluidic channels (1.1 nm for TFP-TPA and 100 nm for ANM) in TFP-TPA COF@ANM [50,51]. For example, at neutral pH, the surface charge densities of TFP-TPA COF and ANM estimated by the Gouy-Chapman equation [52] were about − 5.14 mC/m^2 and 7.18 mC/m^2, respectively. The estimated surface charge density of TFP-TPA

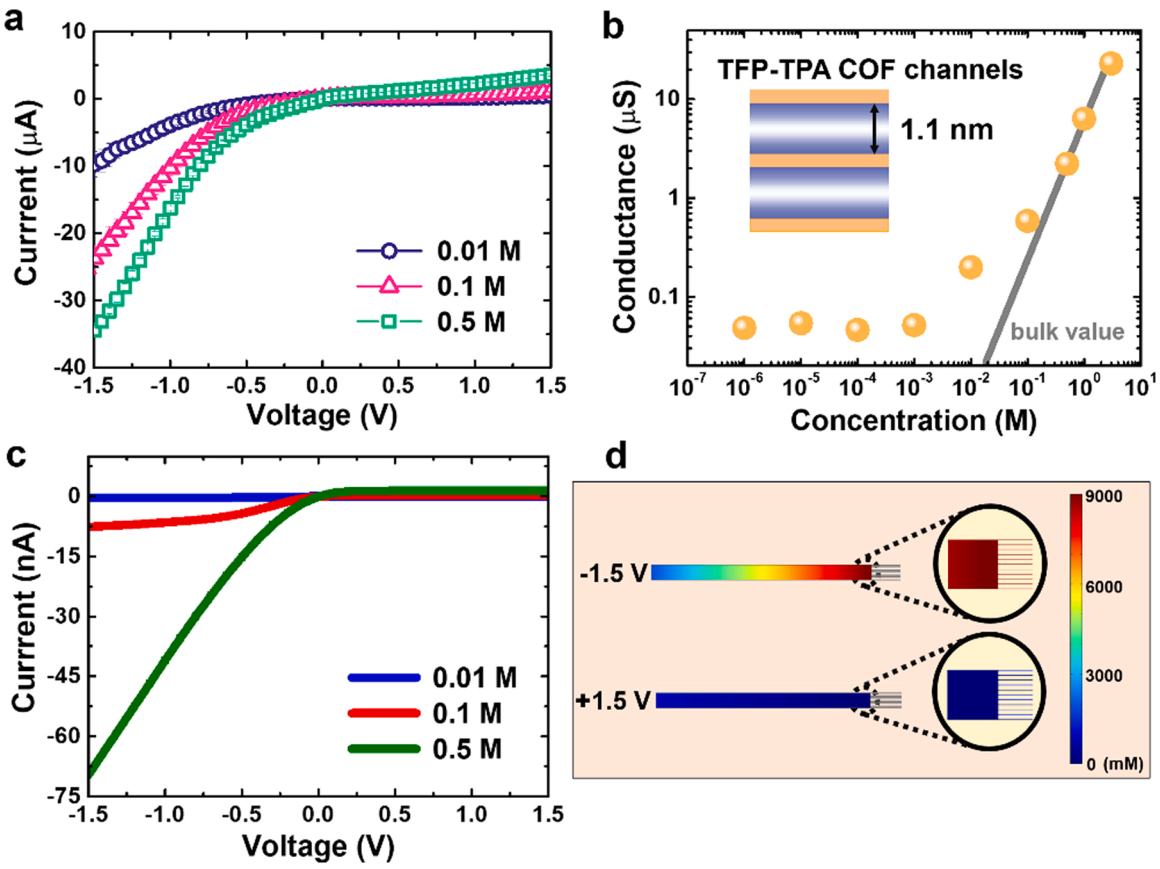

Fig. 3. Highly rectified ion transport. (a) I-V characteristics of TFP-TPA COF@ANM in KCl solutions with various concentrations, revealing apparent diode-like ion transport behavior even in high 0.5 M salt environment. (b) Salt concentration dependence of the transmembrane conductance (circles), which deviates from the bulk property (grey line) from below ~0.5 M, showing a strong surface-charge-governed ion transport property at high salt concentration. Note that at the critical concentration of 0.5 M, the Debye length is ~0.43 nm which is close to the half pore size (0.55 nm, inset) of TFP-TPA COF channels. (c) Numerical modeling of the salt concentration dependent ICR property in the sub-2 nm-scale ionic diode device system under consideration. The solution pH was set at pH 6.2. (d) Simulated result demonstrating the accumulation (–1.5 V) and depletion (+1.5 V) of ions in the considered ionic diode device system. The bulk salt concentration was set at 500 mM.

COF (Fig. S6) is consistent with the previously reported COF-SO_3H in the range of negative 3.2–25.2 mC/m^2 [44], but higher than the $Ti_3C_2T_x$ MXene of − 2.2 mC/m^2 [53]. We then analyzed the salt concentration dependence of transmembrane conductance. As shown in Fig. 3b, the membrane conductance deviates from the bulk value (grey line) at a high electrolyte concentration of 0.5 M, revealing an apparent surface-charge-governed ion transport property [54]. This arises because at such 0.5 M KCl, whose Debye length (~0.43 nm) is comparable to the half pore size of TFP-TPA COF channels (inset in Fig. 3b), and therefore, the channel's surface charges play a role on regulating ion transport [55].

To further provide the evidence featuring the salt concentration dependent ICR property of the proposed sub-2 nm-scale ionic diode membrane, we modeled the current-voltage curves in the heterostructured system at various salt concentrations considered in experiments by using the multi-ion Poisson-Nernst-Planck equations (see details in Experimental section) [56,57]. To save computational cost, we simplified the TFP-TPA COF channels as a channel array of 1.1 nm in size and the ANM as a single nanochannel of 101.1 nm in size (Fig. S7). The surface charge densities of the ANM and TFP-TPA COF channels were set to be 0.08 and − 0.06 C/m^2, respectively [58,59]. As depicted in Fig. 3c, the simulated I-V results agree very well with the experimenta1 findings (Fig. 3a). The origin of ICR property can be supported by the voltage-dependent enrichment (−1.5 V) and depletion of ions in the heterostructured system considered (Fig. 3d). Notably, the simulated rectification ratio shows a local maximum dependence on salt concentration, which is also consistent with the experimental results (Fig. S8) and can be explained by the effect of the competition bewteen the Debye length screening and amount of depleted/enriched ions in the confined space [60].

The features of highly rectified and strong surface-charge-governed ion transport property observed in TFP-TPA COF@ANM (Fig. 3) indicates its potential in harvesting energy from salinity gradients. We then investigated the osmotic energy conversion performance by using the same manmade conductive cell (Fig. 4a). Because of the strong ICR effect in TFP-TPA COF@ANM, we first tested the preferential salinity gradient direction, which is advantageous to enhance power output (Fig. 4b). Note that in Fig. 4b, the working electrode was put in the high-concentration reservoir, and the electrode calibration has been carried out by subtracting the contribution of the redox potential [27] (Fig. S9 and S10; details in Supporting Information), so that the intercepts of I-V curves on the voltage- and current-axes are the pure salinity gradient-driven diffusion potential (V_{diff}) and diffusion current (I_{diff}), respectively. In the experiments, we fixed the high-salinity compartment facing the TFP-TPA COF side and the low-salinity compartment facing the ANM side (Fig. 4a), because of a significant decrease of ~67.7% (from 24.3 to 7.86 kΩ) in internal resistance under this salinity gradient configuration (Fig. 4b), advantageous to promoting power output. A decrease of the internal resistance results from the strong ionic rectification of the developed heterogeneous membrane, which causes the preferential direction for cation transport under this salinity gradient direction. The observation is consistent with the earlier reports of ionic

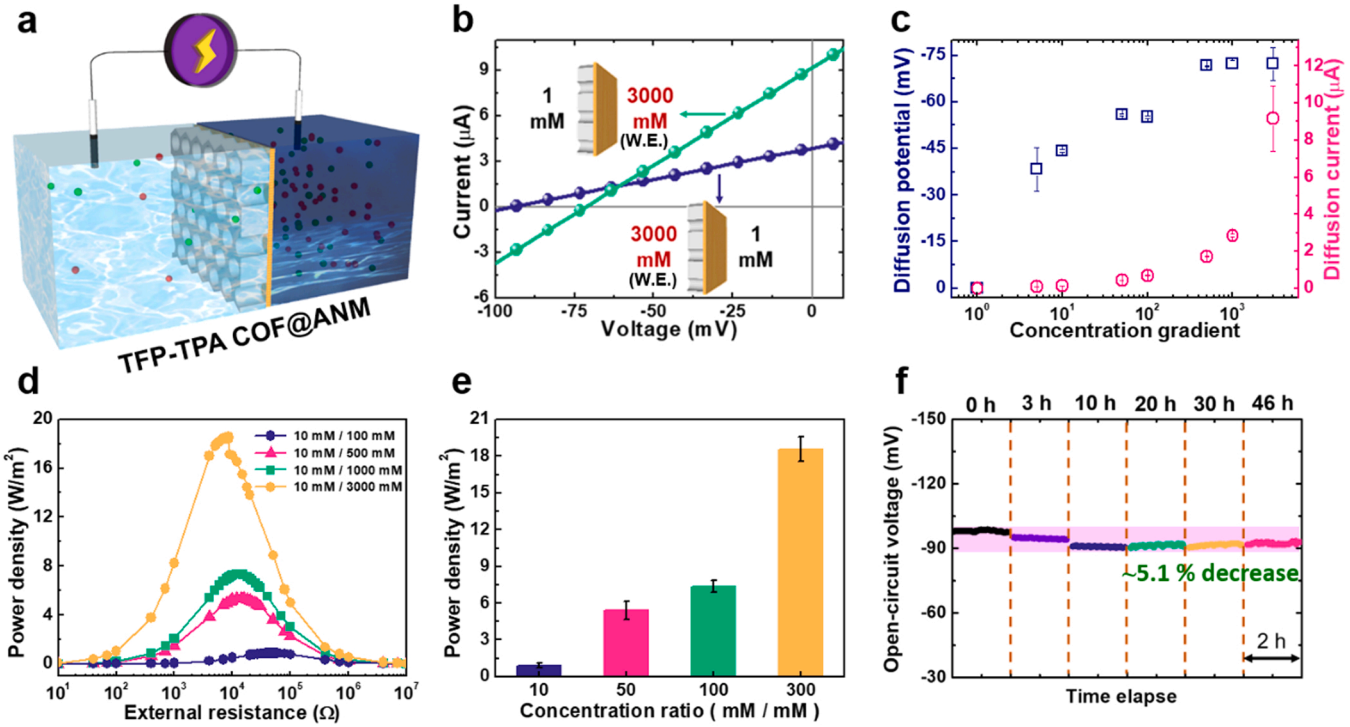

Fig. 4. High-performance osmotic energy harvesting. (a) Schematic of the osmotic energy conversion device used. (b) Two reversed directions of a salinity gradient were tested for osmotic energy harvesting. The I-V curves presented were the pure salinity gradient-driven results because the contribution of the redox potential at the electrodes has been subtracted. Thus, the intercepts on the voltage-axis and current-axis are the diffusion potential (V_{diff}) and diffusion current (I_{diff}), respectively. (c) The generated V_{diff} and I_{diff} as a function of salinity gradient. The low-concentration was fixed at 1 mM in the ANM-side reservoir. (d) Osmotic power harvested under various salinity gradients. The power densities achieved were ca. 0.91, 5.41, 7.38, and 18.6 W/m^2 at the 10-fold, 50-fold, 100-fold and 300-fold salinity gradients, respectively. (e) The power density outputted by TFP-TPA COF@ANM as a function of salinity gradient. (f) Stability test. The V_{oc} was recorded under a 0.5 M/0.01 M salinity gradient for continuous 48 h without replenishment of electrolyte.

diode membranes with nanoscale channels [27–29]. Fig. 4c summarizes the variations of V_{diff} and I_{diff} with KCl concentration gradients. The values of V_{diff} (I_{diff}) increase from − 38.2 to − 72.3 mV (0.077–9.16 μA) as the concentration increases from 5-fold to 3000-fold, which is expected due to the increase in the driving force for osmotic ion transport. Moreover, the corresponding cation selectivity and energy conversion efficiency decrease from 0.976% to 0.690% and 45.3–7.22%, respectively, estimated from Eq. (S2) and (S3) in Supporting Information (Fig. S11 and Table S1). A sharp increase in diffusion current at high salinity gradient (Fig. 4c) implies the potential of using the exploited sub-2 nm-scale ionic diode membrane in harvesting osmotic energy in hypersaline environments, as will be shown later.

To estimate the practical power output, we transferred the harvested osmotic power to an external circuit equipped with an electrical load (R_l) [27,35]. The generated power can be evaluated as $I^2 \times R_l$, where I is the measured current. The approach we used to identify the practical power output is the same as that employed in the previous reports for the porous membranes, but is different from the method used for the single-pore membranes [7,61], where the contribution of the redox potential was deducted and the pure osmosis-driven power was then estimated. For the porous membranes, significant pore and pore interaction will cause severe ion concentration polarization (ICP) and the increase of the access resistance at the membrane-liquid interfaces, leading to the decrease of pure osmotic power [62]. To enable fair comparison, we used the same approach employed for the porous membranes in later discussion. As expected, the measured current density decreases with an increase of external resistance (Fig. S12), leading to a local maximum dependence of the power density on external resistance (Fig. 4d). As shown in Fig. 4d-e, the power densities outputted by TFP-TPA COF@ANM were about 0.91, 5.41, 7.38, 18.6 W/m^2 under the 10-, 50-, 100-, and 300-fold salinity gradients, respectively. Notably, at the 50-fold salinity gradient simulating the condition where the seawater is mixed with river water, the achieved power output of 5.41 W/m^2 is across the commercial benchmark value (5 W/m^2) [63]. Apparently, the enhancement of the osmotic energy harvesting efficiency of using TFP-TPA COF@ANM can be attributed to its significant ionic diode effect. To demonstrate this, we compared the osmotic energy harvesting efficiency from TFP-TPA COF@ANM with the pure TFP-TPA COF membrane and ANM, both of which did not show ICR property, indicating the ~209% and ~85% enhancements in output power, respectively (Fig. S13). The presence of the ANM in TFP-TPA COF@ANM not only provides ordered aligned channels for facilitating ion transport but also induces strong ionic diode effect, thus leading to amplified power output. Note that the output power of ANM is higher than that of pure TFP-TPA COF membrane, which is due to the fact that the larger pore size of ANM has higher ionic flux and lower resistance (Fig. S14). We also tested the stability of osmotic energy conversion with TFP-TPA COF@ANM by measuring the open-circuit voltage for two days. As shown in Fig. 4 f, only a slightly ~5.1% decrease can be observed through the entire measurement, indicating a high energy generation stability of the developed sub-2 nm-scale COF-based ionic diode membrane.

As shown above, the developed high-performance ionic diode membrane is based on the sub-2 nm COF channels, which endow the membrane with high ability to screen and rectify ions in high saline environments. This drives us to think the possibility of using the TFP-TPA COF@ANM to harvest osmotic energy between the hypersaline salt-lake (5 M NaCl) and river water (0.01 M NaCl) with enhanced efficiency. We thus tested the osmotic energy conversion in such 500-fold salinity gradient at various pH environments. As shown in Fig. 5a and S15, the TFP-TPA COF@ANM can reach ca. 24.9, 27.8, and 31.3 W/m^2 at pH 3.2, 6.2 and 10, respectively. Under the pH values considered, the

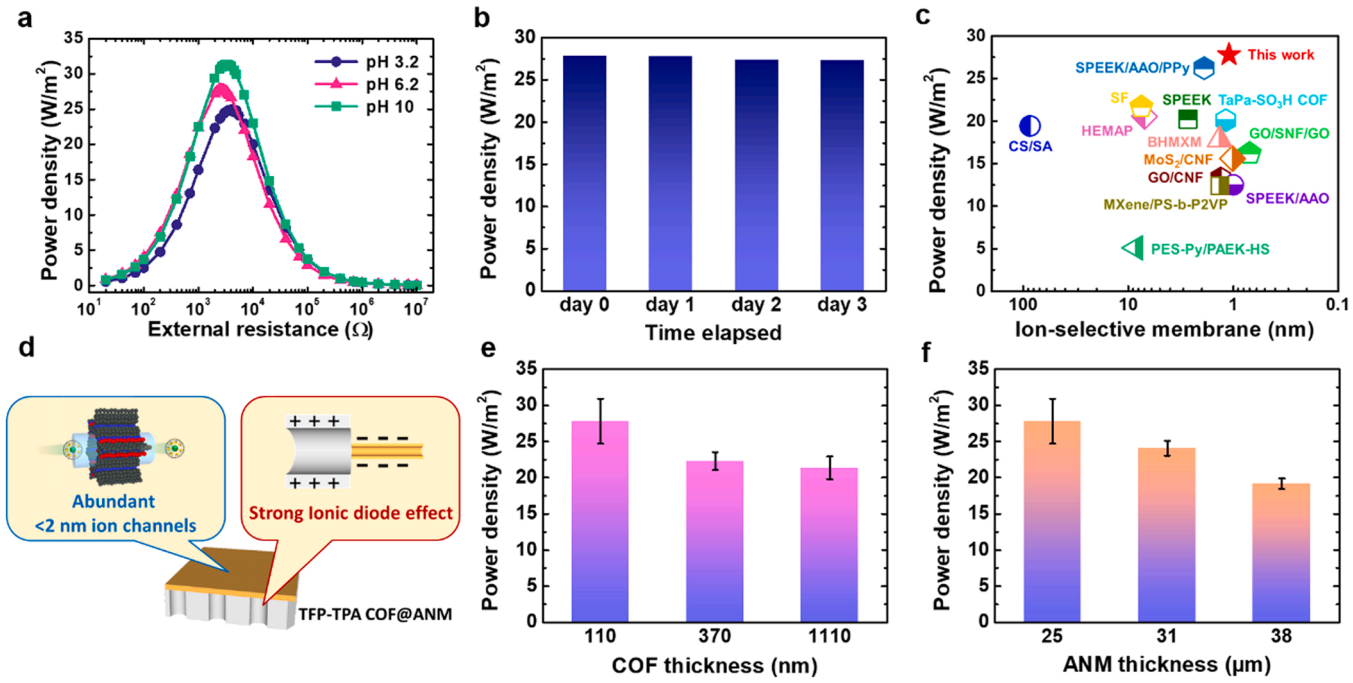

Fig. 5. Ultrahigh osmotic power generation in the hypersaline condition (5 M/0.01 M NaCl gradient). (a) Osmotic power harvested at the mixing of artificial salt-lake water and river water (500-fold NaCl gradient) under various pH values. The power densities achieved were ca. 24.9, 27.8, 31.3 W/m^2 at pH 3.2, 6.2 and 10, respectively. (b) Osmotic energy conversion efficiency of TFP-TPA COF@ANM measured for continuous three days. (c) Comparison of the power densities generated by the TFP-TPA COF@ANM and reported state-of-the-art ion-selective membranes [40,53,64–74] at the same testing conditions (i.e., 500-fold NaCl gradient and 0.03 mm^2 testing area). (d) Schematic diagram of the mechanism underlying the significantly enhanced osmotic energy harvesting with the developed sub-2-nm-scale ionic diode membrane. Influences of the (e) COF thickness and (f) ANM thickness on the osmotic energy conversion efficiency.

achieved power densities are all higher than the bottleneck (20 W/m^2) reported from most of previous state-of-the-art membranes [40,53, 64–74] (Table S2), indicating high-performance osmotic energy harvesting over a wide pH range. The images and PXRD patterns shown in Fig. S16 and BET surface area measurements (Table S3) also proved that the prepared TFP-TPA COF membrane had a strong tolerance in acidic, basic and hypersaline environments, owing to the strong covalent bonds in molecules. Fig. 5b and S17 also showed that only 1.8% decrease (from 27.8 to 27.3 W/m^2) of output power density can be observed when the TFP-TPA COF@ANM was employed in osmotic power generation for continuous 3 days, revealing its high stability in energy conversion. Note especially at neutral condition (pH 6.2) that, an unprecedented power density of 27.8 W/m^2 has been achieved, which outperforms all the reported values under the same testing condition (Fig. 5c). Compared with earlier studies with similar heterogeneous membranes [27–34], this is the first one reporting the assembly of sub-2 nm COF channels in an ionic diode membrane for amplified osmotic energy conversion. It is thus concluded that benefiting from a large number of aligned sub-2-nm ion channels in TFP-TPA COF and highly ordered nanochannels in ANM, and strong ionic diode effect in the resulting heterogeneous membrane (Fig. 5d), the developed COF-based sub-2 nm-scale ionic diode membrane is capable of achieving highly efficient osmotic energy harvesting especially in hypersaline environments.

Furthermore, we also tested the effects of the COF and ANM thicknesses on the osmotic power generation performance of TFP-TPA COF@ANM under a 500-fold NaCl gradient. The COF thickness was regulated by increasing the interfacial synthesis time. Fig. S18 reveals that the COF thickness can be increased to 370 and 1110 nm for 4 and 10 days of the synthesis time, respectively. As shown in Fig. 5e and S19, the increase of COF thickness resulted in the decrease of output power density. This dependence can be attributed to the increase of membrane resistance, which hinders ion transport. Similar behavior can be found in the ANM thickness-dependent osmotic power shown in Fig. 5d and S20. The thicker the ANM thickness the larger the membrane resistance, leading to the smaller the output power. Fig. S21 shows the testing area effect on the osmotic power generation performance of TFP-TPA COF@ANM. The achieved power densities were about 27.8, 8.61, and 2.27 W/m^2 when using the testing area of 0.03, 0.196, and 0.785 mm^2, respectively. The decreasing power output with increasing effective testing area is consistent with earlier reports [64,75,76] and attributed to the more significant pore and pore interaction and ICP effects, which result in higher access resistance and smaller transmembrane concentration gradient [62]. Note that due to the reduced ICP effect from the use of an ionic diode membrane, the power density of 8.61 W/m^2 realized at a larger testing area of 0.196 mm^2 still reaches a high performance level, compared with the previously reported value (< 2 W/m^2) [64].

To further provide more physical insights in ultrahigh osmotic power generation of the sub-2 nm system considered, we modeled osmotic ion transport in the TFP-TPA COF@ANM and ANM in a 5 M/0.01 M NaCl gradient. The pH-dependent surface charge densities of the COF channels and ANM channel assumed in the modeling can be found in Table S4, in accordance with the charge natures of TFP-TPA COF (Fig. S6) and ANM [48,77]. Fig. 6a-b suggests that the severe ICP effect occurs in the sub-2 nm TFP-TPA COF channel region, thus leading to promotion (demotion) of total ion concentration at the high-concentration (low-concentration) entrance of the TFP-TPA COF@ANM, as compared with the ANM system (Fig. S22). This results in a huge ~191% enhancement (from 10.21-fold for ANM to 29.75-fold for TFP-TPA COF@ANM) of the effective salinity ratio (ESR), which is the major driving force dominating the osmotic power generation performance [25], in the TFP-TPA COF@ANM system. Moreover, the TFP-TPA COF@ANM possesses higher selectivity to counterions due to the presence of sub-2 nm COF channels (Fig. 6c). The net effects of the strong ionic diode effect (as verified in Fig. 3), higher ESR driving force, and higher ion selectivity endow the developed sub-2 nm-scale ionic diode membrane (TFP-TPA COF@ANM) with ultrahigh osmotic power. More notably, the estimated ESR value in the TFP-TPA COF@ANM is

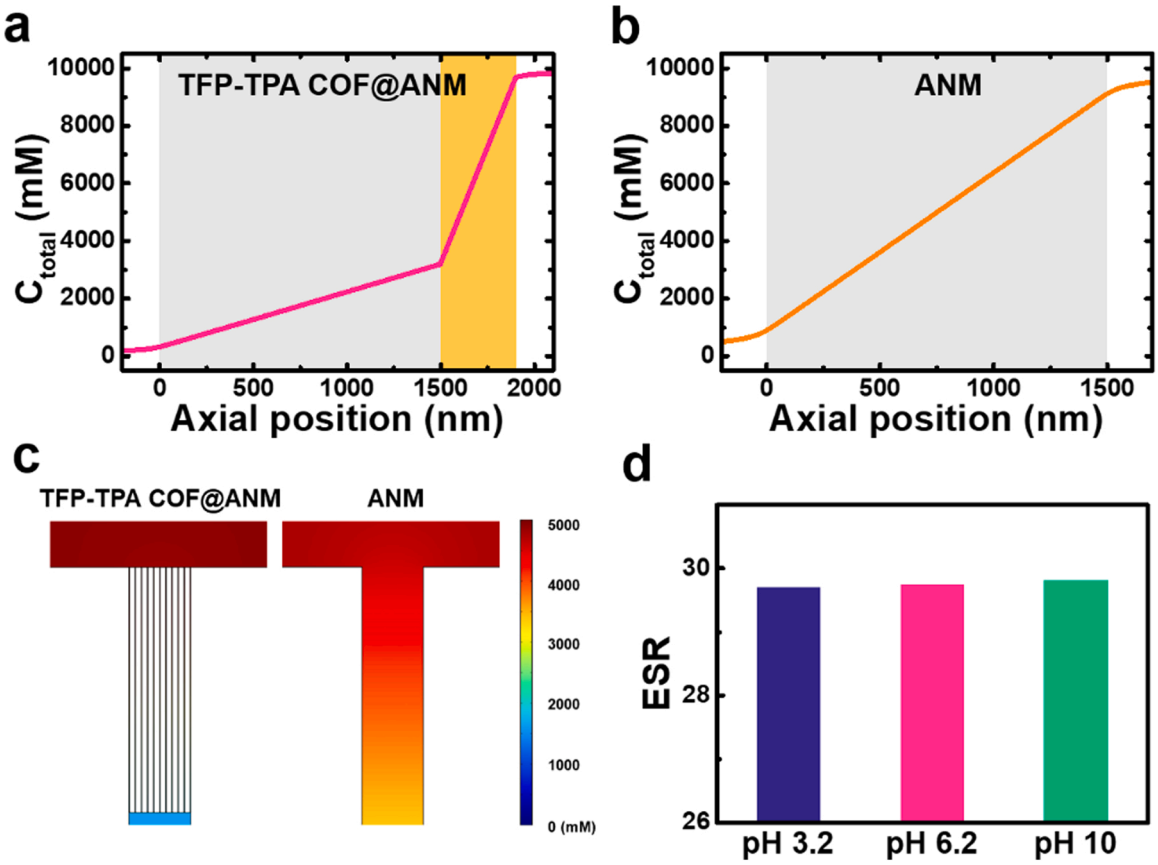

Fig. 6. Numerical simulation of osmotic ion transport properties. Simulated axial variations of the total ion concentration (C_{total}) in (a) TFP-TPA COF@ANM and (b) ANM at pH 6.2. The grey and orange regions highlight the interiors of ANM and TFP-TPA COF, respectively. The effective salinity ratios (ESR), which were calculated as the ratio of C_{total} at the high-concentration and low-concentration entrances, for TFP-TPA COF@ANM and ANM are 29.75 and 10.21-fold, respectively. (c) Contours of the counterion concentration near the high-concentration entrance of TFP-TPA COF@ANM and ANM. (d) Estimated ESR as a function of pH value. Here, the bulk concentration gradient of NaCl was set as 5 M and 0.01 M, as those employed in Fig. 5.

nearly independent on pH (surface charge natures of TFP-TPA COF and ANM channels) and maintains at a relatively high level, as compared to the ANM (Fig. 6d and S23). This implies the importance of the assembly of the aligned sub-2 nm channels in an ionic diode membrane and explains why the TFP-TPA COF@ANM is capable of achieving ultrahigh osmotic power over a wide pH range (Fig. 5a). This also suggests the importance of the incorporation of aligned sub-2 nm channels into the design of high-performance ionic diode membranes in practical applications of osmotic energy harvesting.

3. Conclusion

In summary, we have developed a bioinspired sub-2 nm-scale ionic diode membrane (TFP-TPA COF@ANM), composed of an ultrathin TFP-TPA COF membrane and a highly ordered ANM, for highly efficient osmotic energy harvesting. Our experimental and simulation results prove that the asymmetric surface charges and pore sizes (1.1 nm for TFP-TPA COF and 100 nm for ANM) of two aligned channels in the heterogeneous membrane we built endow it with high ionic rectification even in high 0.5 M salt concentration. Benefiting from the strong ionic diode effect and abundant sub-2 nm ion channels, the developed membrane, at the condition at which the synthetic salt-lake water (5 M NaCl) and river water (0.01 M NaCl) is mixed, can reach a record power output of 27.8 W/m^2, outperforming all the state-of-the-art membranes under the same testing condition. This proof-of-concept research paves a new way of using the rectified ion channel-mimetic membrane to realize fabulous osmotic power generation.

4. Experimental section

4.1. Fabrication of ANM

The alumina nanochannel membrane (ANM) with highly ordered straight channel arrays was fabricated by the two-step anodization process, modified from our previous study [35]. First, a high purity aluminum (Al, 99.9995%) sheet was washed with acetone, ethanol, and water in sequence and then electrochemically polished with the $HClO_4$/ethanol solution (1:4, v/v) under 20 V for 90 s. The first anodization was carried out in 0.3 M oxalic acid under 50 V at 20 °C for 30 min. Then, the disordered oxide layer was removed using the mixed solution (H_3PO_4/CrO_3/water) at 60 °C for 90 min. The second anodization was performed under the same condition of first anodization for 1 h, followed by the pore widening process with 5 wt% phosphoric acid. To obtain a free-standing ANM support, the remaining Al was removed by the mixed solution ($CuCl_2$/HCl/water), followed by the etching of barrier layer carried out by 5 wt% H_3PO_4 for 1 h at 30 °C.

4.2. Fabrication of TFP-TPA COF@ANM

The continuous TFP-TPA COF membrane was fabricated via interfacial polymerization of 1,3,5-triformylphloglucinol (TFP) and tris(4-aminophenyl)amine (TPA-3NH_2), as depicted in Fig. 1b. The TFP (15.8 mg, 0.073 mmol) was first dissolved into 100 mL of dichloromethane in glass beaker, followed by addition of 60 mL of deionized water on the top of TFP solution. The resulting aqueous-organic layered solution was sonicated for 5 min to release dissolved air bubbles. Then, a

solution of TPA-3NH_2 (21.8 mg, 0.075 mmol) and p-toluenesulfonic acid (65 mg, 0.377 mmol) in 70 mL of deionized water and 30 mL of acetonitrile was gently placed on the above-mentioned aqueous-organic solution. The resulting layered solution was kept at room temperature for 2 days. The formed TFP-TPA COF membrane at the aqueous-organic solution interface was then rinsed with water and acetone several times for 1 h to remove any residual monomers. Finally, the TFP-TPA COF@ANM was prepared by transferring the above TFP-TPA COF membrane onto the ANM, followed by the thermal annealing at 80 ºC for 3 days in oven.

4.3. Characterizations

The SEM images were captured on a JEOL JSM-7900 F operating at an accelerating voltage of 5 kV. The HRTEM image was captured on a field emission gun TEM (FEI Tecnai G2 F30) operating at a voltage of 300 kV. PXRD patterns were measured on a Simens D5000 at room temperature with monochromated Cu Kα radiation ($\lambda = 0.1542$ nm). TFP-TPA COF membranes were first grinded into powders and then tested in the 2θ degree of 4–40°. FTIR spectra were recorded using a Bruker Tensor 27 FTIR spectrophotometer. Contact angle measurements were measured on a contact angle instrument OSA60-G (Ningbo NB Scientific Instruments Co., Ltd., China). BET surface area and pore size distribution of as-grinded TFP-TPA COF powders were analyzed by measuring N_2 adsorption/desorption isotherms at 77 K using a Micromeritics ASAP 2020 Surface Area and Porosity analyzer. Solid state NMR spectrum of TFP-TPA COF membrane was recorded using a Bruker Avance 400 NMR spectrometer and a Bruker magic angle spinning (MAS) probe, running 32,000 scans. Cross-polarization with MAS (CPMAS) was used to acquire ^{13}C NMR spectral data at 75.5 MHz. The zeta potential measurements were performed using the Zetasizer Nano ZS (Malvern Instruments, UK) in 0.01 M KCl solutions with various pH values.

4.4. Electrical measurement

Ion transport property and osmotic energy conversion of all membranes, which were mounted between two-compartments of a manmade conductive cell, were tested using Keithley 6487 picoammeter and a pair of manmade Ag/AgCl electrodes. The working electrode was placed in the compartment facing the COF side, while the other side was grounded. For ion transport tests, the voltage changed from − 1.5 V to + 1.5 V with 0.05 V steps was applied. For osmotic ion transport tests, all the current-voltage (I-V) curves presented are the pure osmosis driven results because the contribution of the redox potential, which was obtained by measuring the potential drop of a non-ion-selective micro-hole silicon wafer without TFP-TPA COF@ANM, has been subtracted. To measure the practical power output, an external load resistor (RS-200, IET Labs Inc.) was connected to the electrochemical cells through a pair of Ag/AgCl electrodes (Fig. S24), which is the same measurement method, as used in the publications listed in Table S2 [40,53,64–74]. The testing area for ion transport was 0.03 mm^2, the same as employed in previous publications [40,53,64–74].

4.5. Multiphysics simulation

Ion transport property of the heterostructured COF/ANM channel system under consideration was modeled by solving the multi-ion Poisson-Nernst-Planck equations (see details in our previous studies [56,57]) using the commercial finite element software, COMSOL Multiphysics 4.3a. To simulate the practical condition, we considered four kinds of ionic species, namely, K^+ (or Na^+), Cl^-, H^+, and OH^-. To save computational cost, we simplified the COF channels as a nanochannel array of 1.1 nm in diameter and 400 nm in length and the ANM as a nanochannel of 101.1 nm in size and 1500 nm in length (Fig. S7). The heterostructured COF/ANM channel system was connected to two identical large reservoirs. Because the simulated system is at the sub-2 nm-scale, the effect of electroosmotic flow [78] was neglected in the modeling. The pH dependent surface charge densities of COF channels and ANM channel used in the modeling can be found in Table S4. For example, at pH 6.2, we assumed the surface charge density of COF channels is -0.06 C/m^2 and that of the ANM channel is 0.08 C/m^2 [58].

CRediT authorship contribution statement

Mengyao Gao: Formal analysis, Investigation, Visualization, Writing – original draft. **Min-Jie Zheng:** Methodology, Investigation, Visualization, Validation, Data curation. **Ahmed F.M. EL-Mahdy:** Validation, Resources, Data curation. **Chen-Wei Chang**: Investigation, Data curation, Software. **Yu-Chun Su**: Investigation, Validation, Data curation. **Wen-Hsin Hung**: Data curation, Software. **Shiao-Wei Kuo:** Conceptualization, Resources, Writing – review & editing, Supervision, Funding acquisition. **Li-Hsien Yeh:** Conceptualization, Methodology, Writing – original draft, Writing – review & editing, Supervision, Project administration, Funding acquisition.

Declaration of Competing Interest

The authors declare that they have no known competing financial interests or personal relationships that could have appeared to influence the work reported in this paper.

Data Availability

Data will be made available on request.

Acknowledgements

This work was financially supported by the National Science and Technology Council, Taiwan under Grants MOST 111-2628-E-011-013, 111-2124-M-002-021, 110-2223-E-011-003-MY3, 110-2124-M-002-013, 108-2628-E-011-006-MY3, and 108-2638-E-002-003-MY2.

Appendix A. Supporting information

Supplementary data associated with this article can be found in the online version at doi:10.1016/j.nanoen.2022.108007.

References

[1] M. Macha, S. Marion, V.V.R. Nandigana, A. Radenovic, 2D materials as an emerging platform for nanopore-based power generation, Nat. Rev. Mater. 4 (2019) 588–605.
[2] Z. Zhang, L.P. Wen, L. Jiang, Nanofluidics for osmotic energy conversion, Nat. Rev. Mater. 6 (2021) 622–639.
[3] A. Siria, M.L. Bocquet, L. Bocquet, New avenues for the large-scale harvesting of blue energy, Nat. Rev. Chem. 1 (2017) 0091.
[4] S. Balme, T.J. Ma, E. Balanzat, J.M. Janot, Large osmotic energy harvesting from functionalized conical nanopore suitable for membrane applications, J. Membr. Sci. 544 (2017) 18–24.
[5] C.C. Yu, X.B. Zhu, C.Y. Wang, Y.H. Zhou, X.T. Jia, L. Jiang, X. Liu, G.G. Wallace, A. Smart, Cyto-compatible asymmetric polypyrrole membrane for salinity power generation, Nano Energy 53 (2018) 475–482.
[6] L.H. Yeh, Z.Y. Huang, Y.C. Liu, M.J. Deng, T.H. Chou, H.C.O. Yang, T. Ahamad, S. M. Alshehri, K.C.W. Wu, A nanofluidic osmotic power generator demonstrated in polymer gel electrolytes with substantially enhanced performance, J. Mater. Chem. A 7 (2019) 26791–26796.
[7] T.J. Ma, E. Balanzat, J.M. Janot, S. Balme, Nanopore functionalized by highly charged hydrogels for osmotic energy harvesting, ACS Appl. Mater. Interfaces 11 (2019) 12578–12585.
[8] V.P. Mai, R.J. Yang, Boosting power generation from salinity gradient on high-density nanoporous membrane using thermal effect, Appl. Energy 274 (2020), 115294.
[9] X. Liu, M. He, D. Calvani, H.Y. Qi, K. Gupta, H.J.M. de Groot, G.J.A. Sevink, F. Buda, U. Kaiser, G.F. Schneider, Power generation by reverse electrodialysis in a single-layer nanoporous membrane made from core-rim polycyclic aromatic hydrocarbons, Nat. Nanotechnol. 15 (2020) 307–312.

[10] Y.D. Wu, Y.C. Qian, B. Niu, J.J. Chen, X.F. He, L.S. Yang, X.Y. Kong, Y.F. Zhao, X. B. Lin, T. Zhou, L. Jiang, L.P. Wen, Surface charge regulated asymmetric ion transport in nanoconfined space, Small 17 (2021), 2101099.
[11] K. Yazda, K. Bleau, Y.N. Zhang, X. Capaldi, T. St-Denis, P. Grutter, W.W. Reisner, High osmotic power generation via nanopore arrays in hybrid hexagonal boron nitride/silicon nitride membranes, Nano Lett. 21 (2021) 4152–4159.
[12] L. Ding, D. Xiao, Z.H. Zhao, Y.Y. Wei, J. Xue, H.H. Wang, Ultrathin and ultrastrong kevlar aramid nanofiber membranes for highly stable osmotic energy conversion, Adv. Sci. (2022), 2202869.
[13] V.P. Mai, W.H. Huang, R.J. Yang, EnhancingIon transport through nanopores in membranes for salinity gradient power generation, ACS Es &T Eng. 1 (2021) 1725–1752.
[14] Y. Ma, L.H. Yeh, C.Y. Lin, L.J. Mei, S.Z. Qian, pH-regulated ionic conductance in a nanochannel with overlapped electric double layers, Anal. Chem. 87 (2015) 4508–4514.
[15] W.W. Xin, L. Jiang, L.P. Wen, Two-dimensional nanofluidic membranes toward harvesting salinity gradient, Power, Acc. Chem. Res 54 (2021) 4154–4165.
[16] Z. Zhang, S. Yang, P.P. Zhang, J. Zhang, G.B. Chen, X.L. Feng, Mechanically strong MXene/Kevlar nanofiber composite membranes as high-performance nanofluidic osmotic power generators, Nat. Commun. 10 (2019) 2920.
[17] C.R. Wu, T.L. Xiao, J.D. Tang, Q.Q. Zhang, Z.Y. Liu, J.B. Liu, H. Wang, Biomimetic temperature-gated 2D cationic nanochannels for controllable osmotic power harvesting, Nano Energy 76 (2020), 105113.
[18] L. Ding, D. Xiao, Z. Lu, J.J. Deng, Y.Y. Wei, J. Caro, H.H. Wang, Oppositely charged Ti3C2Tx MXene membranes with 2D nanofluidic channels for osmotic energy harvesting, Angew. Chem. -Int. Ed. 59 (2020) 8720–8726.
[19] L. Cao, H. Wu, C.Y. Fan, Z.M. Zhang, B.B. Shi, P.F. Yang, M. Qiu, N.A. Khan, Z. Y. Jiang, Lamellar porous vermiculite membranes for boosting nanofluidic osmotic energy conversion, J. Mater. Chem. A 9 (2021) 14576–14581.
[20] J. Xu, D.A. Lavan, Designing artificial cells to harness the biological ion concentration gradient, Nat. Nanotechnol. 3 (2008) 666–670.
[21] Z.S. Siwy, Ion-current rectification in nanopores and nanotubes with broken symmetry, Adv. Funct. Mater. 16 (2006) 735–746.
[22] Z. Zeng, Y. Ai, S. Qian, pH-regulated ionic current rectification in conical nanopores functionalized with polyelectrolyte brushes, Phys. Chem. Chem. Phys. 16 (2014) 2465–2474.
[23] C.Y. Lin, T.J. Ma, Z.S. Siwy, S. Balme, J.P. Hsu, Tunable current rectification and selectivity demonstrated in nanofluidic diodes through kinetic functionalization, J. Phys. Chem. Lett. 11 (2020) 60–66.
[24] C.Y. Lin, C. Combs, Y.S. Su, L.H. Yeh, Z.S. Siwy, Rectification of concentration polarization in mesopores leads to high conductance ionic diodes and high performance osmotic power, J. Am. Chem. Soc. 141 (2019) 3691–3698.
[25] J.P. Hsu, T.C. Su, P.H. Peng, S.C. Hsu, M.J. Zheng, L.H. Yeh, Unraveling the anomalous surface-charge-dependent osmotic power using a single funnel-shaped nanochannel, ACS Nano 13 (2019) 13374–13381.
[26] G. Laucirica, M.E. Toimil-Molares, C. Trautmann, W. Marmisoll, O. Azzaroni, Polyaniline for improved blue energy harvesting: highly rectifying nanofluidic diodes operating in hypersaline conditions via one-step functionalization, ACS Appl. Mater. Interfaces 12 (2020) 28148–28157.
[27] J. Gao, W. Guo, D. Feng, H.T. Wang, D.Y. Zhao, L. Jiang, High-performance ionic diode membrane for salinity gradient power generation, J. Am. Chem. Soc. 136 (2014) 12265–12272.
[28] S. Zhou, L. Xie, X.F. Li, Y.A. Huang, L.P. Zhang, Q.R. Liang, M. Yan, J. Zeng, B. L. Qiu, T.Y. Liu, J.Y. Tang, L.P. Wen, L. Jiang, B. Kong, Interfacial super-assembly of ordered mesoporous carbon-Silica/AAO hybrid membrane with enhanced permselectivity for temperature- and pH-Sensitive smart ion transport, Angew. Chem. -Int. Ed. 60 (2021) 26167–26176.
[29] W.W. Xin, Z. Zhang, X.D. Huang, Y.H. Hu, T. Zhou, C.C. Zhu, X.Y. Kong, L. Jiang, L. P. Wen, High-performance silk-based hybrid membranes employed for osmotic energy conversion, Nat. Commun. 10 (2019) 3876.
[30] X.B. Zhu, Y.H. Zhou, J.R. Hao, B. Bao, X.J. Bian, X.Y. Jiang, J.H. Pang, H.B. Zhang, Z.H. Jiang, L. Jiang, A Charge-density-tunable three/two-dimensional polymer/graphene oxide heterogeneous nanoporous membrane for ion transport, ACS Nano 11 (2017) 10816–10824.
[31] X. Sui, Z. Zhang, C. Li, L.C. Gao, Y. Zhao, L.J. Yang, L.P. Wen, L. Jiang, Engineered nanochannel membranes with diode-like behavior for energy conversion over a wide pH range, ACS Appl. Mater. Interfaces 11 (2019) 23815–23821.
[32] Y. Sun, T.D. Dong, C.X. Lu, W.W. Xin, L.S. Yang, P. Liu, Y.C. Qian, Y.Y. Zhao, X. Y. Kong, L.P. Wen, L. Jiang, Tailoring a Poly(ether sulfone) Bipolar membrane: osmotic-energy generator with high power density, Angew. Chem. -Int. Ed. 59 (2020) 17423–17428.
[33] C.W. Chang, C.W. Chu, Y.S. Su, L.H. Yeh, Space charge enhanced ion transport in heterogeneous polyelectrolyte/alumina nanochannel membranes for high-performance osmotic energy conversion, J. Mater. Chem. A 10 (2022) 2867–2875.
[34] Y.L. Xu, Y.J. Song, F. Xu, TEMPO oxidized cellulose nanofibers-based heterogenous membrane employed for concentration-gradient-driven energy harvesting, Nano Energy 79 (2021), 105468.
[35] Y.C. Liu, L.H. Yeh, M.J. Zheng, K.C.W. Wu, Highly selective and high-performance osmotic power generators in subnanochannel membranes enabled by metal-organic frameworks, Sci. Adv. 7 (2021) eabe9924.
[36] K.X. Chen, L.N. Yao, B. Su, Bionic thermoelectric response with nanochannels, J. Am. Chem. Soc. 141 (2019) 8608–8615.
[37] S.S. Yuan, X. Li, J.Y. Zhu, G. Zhang, P. Van Puyvelde, B. Van der Bruggen, Covalent organic frameworks for membrane separation, Chem. Soc. Rev. 48 (2019) 2665–2681.
[38] K.Y. Geng, T. He, R.Y. Liu, S. Dalapati, K.T. Tan, Z.P. Li, S.S. Tao, Y.F. Gong, Q. H. Jiang, D.L. Jiang, Covalent organic frameworks: design, synthesis, and functions, Chem. Rev. 120 (2020) 8814–8933.
[39] X.G. Liang, Y. Tian, Y.F. Yuan, Y. Kim, Ionic covalent organic frameworks for energy devices, Adv. Mater. 33 (2021), 2105647.
[40] S.H. Hou, W.T. Ji, J.J. Chen, Y.F. Teng, L.P. Wen, L. Jiang, Free-standing covalent organic framework membrane for high-efficiency salinity gradient energy conversion, Angew. Chem. Int. Ed. 60 (2021) 9925–9930.
[41] Z.M. Man, J. Safaei, Z. Zhang, Y.Z. Wang, D. Zhou, P. Li, X.G. Zhang, L. Jiang, G. X. Wang, Serosa-mimetic nanoarchitecture membranes for highly efficient osmotic energy generation, J. Am. Chem. Soc. 143 (2021) 16206–16216.
[42] S.F. Chen, C.J. Zhu, W.P. Xian, X.Y. Liu, X.L. Liu, Q.H. Zhang, S.Q. Ma, Q. Sun, Imparting ion selectivity to covalent organic framework membranes using de novo assembly for blue energy harvesting, J. Am. Chem. Soc. 143 (2021) 9415–9422.
[43] X.H. Zuo, C.J. Zhu, W.P. Xian, Q.W. Meng, Q. Guo, X.C. Zhu, S. Wang, Y.Q. Wang, S.Q. Ma, Q. Sun, Thermo-osmotic energy conversion enabled by covalent-organic-framework membranes with record output power density, Angew. Chem. -Int. Ed. 61 (2022), e202116910.
[44] L. Cao, I.C. Chen, C.F. Chen, D.B. Shinde, X.W. Liu, Z. Li, Z.Y. Zhou, Y.T. Zhang, Y. Han, Z.P. Lai, Giant osmotic energy conversion through vertical-aligned ion-permselective nanochannels in covalent organic framework membranes, J. Am. Chem. Soc. 144 (2022) 12400–12409.
[45] Z. Zhang, P. Bhauriyal, H. Sahabudeen, Z.Y. Wang, X.H. Liu, M. Hambsch, S.C. B. Mannsfeld, R.H. Dong, T. Heine, X.L. Feng, Cation-selective two-dimensional polyimine membranes for high-performance osmotic energy conversion, Nat. Commun. 13 (2022) 3935.
[46] C. Wang, J.D. Tang, L.Y. Li, J.H. Wan, Y.C. Ma, Y.H. Jin, J.B. Liu, H. Wang, Q. Q. Zhang, Ultrathin self-standing covalent organic frameworks toward highly-efficient nanofluidic osmotic energy generator, Adv. Funct. Mater. 32 (2022), 2204068.
[47] C.R. DeBlase, K.E. Silberstein, T.T. Truong, H.D. Abruna, W.R. Dichtel, beta-ketoenamine-linked covalent organic frameworks capable of pseudocapacitive energy storage, J. Am. Chem. Soc. 135 (2013) 16821–16824.
[48] Y.S. Su, S.C. Hsu, P.H. Peng, J.Y. Yang, M.Y. Gao, L.H. Yeh, Unraveling the anomalous channel-length-dependent blue energy conversion using engineered alumina nanochannels, Nano Energy 84 (2021), 105930.
[49] C.Y. Lin, L.H. Yeh, Z.S. Siwy, Voltage-induced modulation of ionic concentrations and ion current rectification in mesopores with highly charged pore walls, J. Phys. Chem. Lett. 9 (2018) 393–398.
[50] T.J. Ma, J.M. Janot, S. Balme, Track-etched nanopore/membrane: from fundamental to applications, Small Methods 4 (2020), 2000366.
[51] L. Ma, Z.W. Li, Z.S. Yuan, C.Z. Huang, Z.S. Siwy, Y.H. Qiu, Modulation of ionic current rectification in ultrashort conical nanopores, Anal. Chem. 92 (2020) 16188–16196.
[52] L.H. Yeh, S. Xue, S.W. Joo, S. Qian, J.P. Hsu, Field effect control of surface charge property and electroosmotic flow in nanofluidics, J. Phys. Chem. C. 116 (2012) 4209–4216.
[53] L. Ding, M.T. Zheng, D. Xiao, Z.H. Zhao, J. Xue, S.Q. Zhang, J. Caro, H.H. Wang, Bioinspired Ti3C2Tx MXene-based ionic diode membrane for high-efficient osmotic energy conversion, Angew. Chem. -Int. Ed. 61 (2022), e202206152.
[54] Y. Ma, Y.S. Su, S.Z. Qian, L.H. Yeh, Analytical model for surface-charge-governed nanochannel conductance, Sens. Actuator B-Chem. 247 (2017) 697–705.
[55] D. Stein, M. Kruithof, C. Dekker, Surface-charge-governed ion transport in nanofluidic channels, Phys. Rev. Lett. 93 (2004), 035901.
[56] L.H. Yeh, M. Zhang, S. Qian, Ion transport in a pH-regulated nanopore, Anal. Chem. 85 (2013) 7527–7534.
[57] L.H. Yeh, F. Chen, Y.T. Chiou, Y.S. Su, Anomalous pH-dependent nanofluidic salinity gradient power, Small 13 (2017), 1702691.
[58] Z. Zhang, X.Y. Kong, K. Xiao, G.H. Xie, Q. Liu, Y. Tian, H.C. Zhang, J. Ma, L.P. Wen, L. Jiang, A bioinspired multifunctional heterogeneous membrane with ultrahigh ionic rectification and highly efficient selective ionic gating, Adv. Mater. 28 (2016) 144–150.
[59] C.J. Zhu, W.P. Xian, Y.P. Song, X.H. Zuo, Y.Q. Wang, S.Q. Ma, Q. Sun, Manipulating charge density in nanofluidic membranes for optimal osmotic energy production density, Adv. Funct. Mater. 32 (2022), 2109210.
[60] L.J. Cheng, L.J. Guo, Nanofluidic diodes, Chem. Soc. Rev. 39 (2010) 923–938.
[61] M.Y. Gao, P.C. Tsai, Y.S. Su, P.H. Peng, L.H. Yeh, Single mesopores with high surface charges as ultrahigh performance osmotic power generators, Small 16 (2020), 2006013.
[62] J. Gao, X.L. Liu, Y.N. Jiang, L.P. Ding, L. Jiang, W. Guo, Understanding the giant gap between single-pore- and membrane-based nanofluidic osmotic power generators, Small 15 (2019), 1804279.
[63] X. Tong, S. Liu, J. Crittenden, Y.S. Chen, Nanofluidic membranes to address the challenges of salinity gradient power harvesting, ACS Nano 15 (2021) 5838–5860.
[64] G.S. Bian, N. Pan, Z.H. Luan, X. Sui, W.X. Fan, Y.Z. Xia, K.Y. Sui, L. Jiang, Anti-swelling gradient polyelectrolyte hydrogel membranes as high-performance osmotic energy generators, Angew. Chem. Int. Ed. 60 (2021) 20294–20300.
[65] X.B. Zhu, J.R. Hao, B. Bao, Y.H. Zhou, H.B. Zhang, J.H. Pang, Z.H. Jiang, L. Jiang, Unique ion rectification in hypersaline environment: a high-performance and sustainable power generator system, Sci. Adv. 4 (2018) eaau1665.
[66] W.P. Chen, Q. Wang, J.J. Chen, Q.R. Zhang, X.L. Zhao, Y.C. Qian, C.C. Zhu, L. S. Yang, Y.Y. Zhao, X.Y. Kong, B.Z. Lu, L. Jiang, L.P. Wen, Improved ion transport and high energy conversion through hydrogel membrane with 3D interconnected nanopores, Nano Lett. 20 (2020) 5705–5713.

[67] J.J. Chen, W.W. Xin, X.Y. Kong, Y.C. Qian, X.L. Zhao, W.P. Chen, Y. Sun, Y.D. Wu, L. Jian, L.P. Wen, Ultrathin and robust silk fibroin membrane for high-performance osmotic energy conversion, ACS Energy Lett. 5 (2020) 742–748.
[68] Y.Y. Zhao, J. Wang, X.Y. Kong, W.W. Xin, T. Zhou, Y.C. Qian, L.S. Yang, J.H. Pang, L. Jiang, L.P. Wen, Robust sulfonated poly (ether ether ketone) nanochannels for high-performance osmotic energy conversion, Natl. Sci. Rev. 7 (2020) 1349–1359.
[69] S.H. Hou, Q.R. Zhang, Z. Zhang, X.Y. Kong, B.Z. Lu, L.P. Wen, L. Jiang, Charged porous asymmetric eembrane for enhancing salinity gradient energy conversion, Nano Energy 79 (2021), 105509.
[70] W.W. Xin, H.Y. Xiao, X.Y. Kong, J.J. Chen, L.S. Yang, B. Niu, Y.C. Qian, Y.F. Teng, L. Jiang, L.P. Wen, Biomimetic nacre-like silk-crosslinked membranes for osmotic energy harvesting, ACS Nano 14 (2020) 9701–9710.
[71] Y.D. Wu, W.W. Xin, X.Y. Kong, J.J. Chen, Y.C. Qian, Y. Sun, X.L. Zhao, W.P. Chen, L. Jiang, L.P. Wen, Enhanced ion transport by graphene oxide/cellulose nanofibers assembled membranes for high-performance osmotic energy harvesting, Mater. Horiz. 7 (2020) 2702–2709.
[72] C.C. Zhu, P. Liu, B. Niu, Y.N. Liu, W.W. Xin, W.P. Chen, X.Y. Kong, Z. Zhang, L. Jiang, L.P. Wen, Metallic TWo-dimensional MoS2 composites as high-performance osmotic energy conversion membranes, J. Am. Chem. Soc. 143 (2021) 1932–1940.
[73] X.B. Lin, P. Liu, W.W. Xin, Y.F. Teng, J.J. Chen, Y.D. Wu, Y.F. Zhao, X.Y. Kong, L. Jiang, L.P. Wen, Heterogeneous MXene/PS-b-P2VP NAnofluidic Membranes with Controllable Ion Transport for Osmotic Energy Conversion, Adv. Funct. Mater. 31 (2021), 2105013.
[74] J.R. Hao, B. Bao, J.J. Zhou, Y.S. Cui, X.C. Chen, J.L. Zhou, Y.H. Zhou, L. Jiang, A. Euryhaline-Fish-Inspired, Salinity self-adaptive nanofluidic diode leads to high-performance blue energy harvesters, Adv. Mater. 34 (2022), 2203109.
[75] C. Chen, G.L. Yang, D. Liu, X.G. Wang, N.A. Kotov, W.W. Lei, Aramid nanofiber membranes for energy harvesting from proton gradients, Adv. Funct. Mater. 32 (2022), 2102080.
[76] C. Chen, D. Liu, L. He, S. Qin, J.M. Wang, J.M. Razal, N.A. Kotov, W.W. Lei, Bio-inspired nanocomposite membranes for osmotic energy harvesting, Joule 4 (2020) 247–261.
[77] L.S. Yang, P. Liu, C.C. Zhu, Y.Y. Zhao, M.M. Yuan, X.Y. Kong, L.P. Wen, L. Jiang, Ion transport regulation through triblock copolymer/PET asymmetric nanochannel membrane: model system establishment and rectification mapping, Chin. Chem. Lett. 32 (2021) 822–825.
[78] Y. Ai, M.K. Zhang, S.W. Joo, M.A. Cheney, S. Qian, Effects of electroosmotic flow on ionic current rectification in conical nanopores, J. Phys. Chem. C 114 (2010) 3883–3890.

Dr. Mengyao Gao is a researcher in Department of Chemical Engineering, National Taiwan University of Science and Technology. She received her Ph.D. in Materials Science and Engineering from Beijing University of Chemical Technology in 2016. Her research is mainly focused on blue energy, green materials, negative emissions, lithium-ion batteries, sodium-CO_2 batteries, and stretchable devices.

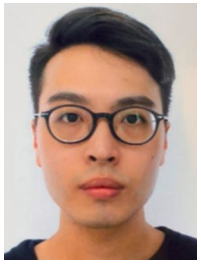

Min-Jie Zheng received his M.S. degree in Department of Chemical Engineering, National Taiwan University of Science and Technology, Taiwan in 2020 under the supervision of Dr. Li-Hsien Yeh. His current research focuses on COF membranes and osmotic energy conversion.

Dr. Ahmed F. M. EL-Mahdy received his Ph.D. degree in Chemistry of Biofunctional Molecules at the Graduate School of Biomedical Sciences, University of Nagasaki in 2014, Japan. He is currently an assistant professor in Chemistry Department, Assiut University, Egypt and Department of Materials and Optoelectronic Science, National Sun Yat-Sen University, Taiwan. His research interests focus on the synthesis of conjugated microporous polymers and covalent organic frameworks for green applications including photocatalysis, energy storage, and biological sensing.

Chen-Wei Chang received his M.S. degree in Department of Chemical Engineering, National Taiwan University of Science and Technology, Taiwan in 2022 under the supervision of Dr. Li-Hsien Yeh. His current research focuses on COF membranes and ionic gradient power.

Yu-Chun Su received her B.C. degree in Department of Chemical and Materials Engineering, National Central University, Taiwan in 2021. She is currently a graduate student under the supervision of Dr. Li-Hsien Yeh at National Taiwan University of Science and Technology, Taiwan. Her current research focuses on nanofluidic energy conversion.

Wen-Hsin Hung received her B.C. degree in Department of Chemical and Materials Engineering, National University of Kaohsiung, Taiwan in 2021. She is currently a graduate student under the supervision of Dr. Li-Hsien Yeh at National Taiwan University of Science and Technology, Taiwan. Her current research interests focus on nanofluidics, ion transport, and energy conversion from salinity gradient.

Dr. Shiao-Wei Kuo received his B.Sc. in chemical engineering from the National Chung Hsing University (1998) and Ph.D. in applied chemistry from the National Chiao Tung University in Taiwan (2002). He continued his research work at Chiao Tung University as a postdoctoral researcher during 2002–2007. Now, he is the chair professor in the Department of Materials and Optoelectronic Science, National Sun Yat-Sen University, Taiwan. His research interests include polymer interactions, self-assembly nanostructures, mesoporous materials, POSS nanocomposites, and polybenzoxazine, and covalent organic framework.

Dr. Li-Hsien Yeh is currently a Full Professor in Department of Chemical Engineering, National Taiwan University of Science and Technology, Taiwan. He received his Ph.D. degree in Chemical Engineering from National Taiwan University, Taiwan in 2007. He was awarded the SCEJ Award for Outstanding Asian Researcher and Engineer from the Society of Chemical Engineers (SCEJ), Japan in 2020. His current research interests include microfluidics and nanofluidics, MOF/COF membranes, ionic circuit, and nanofluidic energy conversion.